

Superfluidity and effective mass of magnetoexcitons in topological insulator bilayers: Effect of inter-Landau-level Coulomb interaction

Zhigang Wang,¹ Zhen-Guo Fu,^{2,1} and Ping Zhang^{1,*}

¹*LCP, Institute of Applied Physics and Computational Mathematics,
P.O. Box 8009, Beijing 100088, People's Republic of China*

²*State Key Laboratory for Superlattices and Microstructures,
Institute of Semiconductors, Chinese Academy of Sciences,
P. O. Box 912, Beijing 100083, People's Republic of China*

The effective mass and superfluidity-normal phase transition temperature of magnetoexcitons in topological insulator bilayers are theoretically investigated. The intra-Landau-level Coulomb interaction is treated perturbatively, from which the effective magnetoexciton mass is analytically discussed. The inclusion of inter-Landau-level Coulomb interaction by more exact numerical diagonalization of the Hamiltonian brings out important modifications to magnetoexciton properties, which are specially characterized by prominent reduction in the magnetoexciton effective mass and promotion in the superfluidity-normal phase transition temperature at a wide range of external parameters.

PACS numbers: 73.21.Ac, 73.22.Pr, 73.30.+y

I. INTRODUCTION

The bilayer n - p systems [1, 2], comprising electrons from the n layer and holes from the p layer, have been the subject of recent theoretical and experimental investigations. These systems, including coupled quantum wells [3–6] and layered graphene [7–13], are of interest, in particular, in connection with the possibility of the Bose-Einstein condensation and superfluidity of indirect excitons or electron-hole pairs. The superfluidity is manifested as nondissipative flow of electric currents, equal in magnitude and opposite in direction, along the layers. In high magnetic fields, two-dimensional excitons survive in a substantially wider temperature range, as the exciton binding energies increase with magnetic field.

Recently, topological insulator (TI) as a new phase of quantum matter, which can not be adiabatically connected to conventional insulators and semiconductors, have been studied intensively [14–23]. Present technological advances have allowed the production of topological insulator bilayers (TIBs) system, which consist of two TI thin films separated by a dielectric barrier. On one hand, CdTe/HgTe TI quantum wells are two-dimensional which are ideal for designing the TIBs, since CdTe/HgTe can be either doped in n -type or p -type [24]; while on the other hand, although the three-dimensional TI Bi₂Se₃ is dominated by charged selenium vacancies, which results in n -type behavior, it could also exhibit p -type behavior by doping method. Transport and magnetic properties of TIs doped by Cr, Fe, and Cu, and n -type to p -type crossover in Bi₂Se₃ codoped with Sb and Pb have been investigated variously in experiments. Recently, in particular, the p -type Bi₂Se₃ single crystal has been ob-

tained by doping Ca in experiments [25]. It is possible to use Al₂O₃ or SiO₂ as the dielectric spacer, on which, remarkably, high-quality Bi₂Se₃ and Bi₂Te₃ TI quantum well thin films have been now successively grown [26–29]. Besides, high quality Bi₂Se₃/ZnSe multilayers [30], and superlattices constructed by alternating Bi₂Se₃ and In₂Se₃ layers [31] have also been successfully obtained in experiments.

TIs are characterized by a full insulating gap in the bulk and protected gapless edge or surface states. It is the gapless edge or surface states that results in the absence of exciton at the TI heterostructures. However, there are various methods, such as introduction of a magnetic exchange field or a strong external magnetic field, to produce a gap in TI heterostructures, which may lead to the formation of excitons [32, 33] or magnetoexcitons. Magnetoexcitons, which have been observed experimentally in semiconductor quantum wells, is an ideal object in exploring the Coulomb interaction effects in TIBs system and Bose-Einstein condensation since it behaves as neutral bosons at low densities. Moreover, as mentioned above, the TIBs, which are required for generating magnetoexcitons, are achievable in current experimental capabilities. Motivated by its importance both from basic point of interest and from application of TI-based electronics, in the present paper we address this issue by presenting an attempt at the theoretical evaluation of superfluidity property and effective mass of magnetoexcitons in the TIBs structure [see Fig. 1(a)] in the presence of a perpendicular high magnetic field, which produces a gap since the Dirac-type energy spectrum becomes discrete by forming Landau levels (LLs).

In the presence of the high magnetic field, the system may exhibit the phase transition from the high-temperature disordered or delocalized phase with the exponential correlation to a low-temperature quasi-ordered or localized phase, which is named as Kosterlitz-Thouless (KT) transition. We study the properties of magnetoex-

*Corresponding author; zhang_ping@iapcm.ac.cn

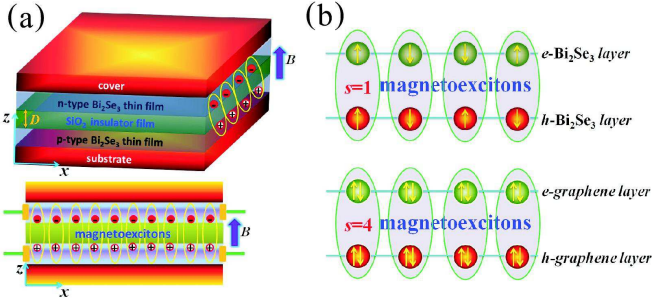


FIG. 1: (Color online) (a) Scheme of TIB comprising two Bi_2Se_3 thin films separated by SiO_2 spacer. Electron (hole) carriers are induced by n (p)-type doping or applied gates. To produce magnetoexcitons a strong perpendicular magnetic field is applied. (b) Illustration of the difference of magnetoexcitons between TIB and graphene bilayer. The spin degeneracy factor $s=4$ in graphene bilayer leads its undressed magnetoexciton mass to be $1/4$ times of that in TIB.

citons in TIBs, including the effective magnetoexciton mass m_B and superfluid-normal state, i.e., KT transition temperature T_c . Comparing to bilayer graphene [11], the effective mass of magnetoexcitons in TIBs is found to be four times larger due to the spin degeneration [see Fig. 1(b)]. Meanwhile, we also investigate the effect of inter-LL Coulomb interaction on the magnetoexciton superfluidity in TIBs, which has been ignored in previous studies on semiconductor and graphene systems. We find that although the intra-LL Coulomb interaction plays the main role in deciding the effective magnetoexciton mass and KT temperature, the inclusion of inter-LL Coulomb interaction brings out important modifications. In fact, at the magnetic field $B=10 \sim 20$ T and the spacer thickness $D=25 \sim 35$ nm in the setup in Fig. 1(a), our results show that the inter-LL Coulomb interaction will reduce the magnetoexciton effective mass by $15\% \sim 25\%$ and improve the KT temperature by $20\% \sim 25\%$.

II. EFFECTIVE MAGNETIC MASS

We start with the effective Hamiltonian of TIB system $H = H_0 + U(r)$, where

$$H_0 = v_F \sigma_e \cdot (\hat{\mathbf{z}} \times \pi_e) - v_F \sigma_h \cdot (\hat{\mathbf{z}} \times \pi_h) \quad (1)$$

is the free electron-hole part of TIB, while $U(r) = -e^2/\epsilon\sqrt{r^2 + D^2}$ is the Coulomb interaction between a pair of electron and hole with $r = r_e - r_h$ being the relative coordinate in the $x - y$ plane and D the spacer thickness. Here, $r_{e(h)}$ represents the position of the electron (hole), and $\pi_{e(h)} = p_{e(h)} \pm eA_{e(h)}/c = -i\partial/\partial r_{e(h)} \pm eA_{e(h)}/c$ denotes the in-plane momentum of the electron (hole), where the gauge is chosen as $A_{e(h)} = B(0, x_{e(h)}, 0)$ in the following calculations. v_F is the Fermi velocity ($\sim 3 \times 10^5$ m/s for Bi_2Se_3 -family materials), $\hat{\mathbf{z}}$ is the unit vector normal to the surface, and $\sigma_e = \sigma \otimes I$ ($\sigma_h = I$

$\otimes \sigma$) describes the spin operator acting on the electron (hole), in which σ denotes a vector of Pauli matrices and I is the 2×2 identity matrix.

The LLs of H_0 are given by

$$E_{n_+, n_-}^{(0)} = \frac{\sqrt{2}v_F}{r_B} [\text{sgn}(n_+) \sqrt{|n_+|} - \text{sgn}(n_-) \sqrt{|n_-|}]. \quad (2)$$

The corresponding eigenstates can be analytically expressed as [10]

$$\psi_{\mathbf{P}}(\mathbf{R}, \mathbf{r}) = \exp \left[i \left(\mathbf{P} + \frac{e}{2c} [\mathbf{B} \times \mathbf{r}] \right) \cdot \mathbf{R} \right] \Psi(\mathbf{r} - \mathbf{r}_0), \quad (3)$$

where $R = (r_e + r_h)/2$ and $r_0 = r_B^2 (\hat{B} \times P)$ with magnetic length $r_B = \sqrt{\hbar c / eB}$ and unit magnetic field \hat{B} . For an electron in LL n_+ and a hole in LL n_- , the four-component wave functions in the relative coordinate are written as

$$\Psi_{n_+, n_-}(\mathbf{r}) = |n_+, n_-\rangle \quad (4)$$

$$= (\sqrt{2})^{\delta_{n_+, 0} + \delta_{n_-, 0} - 2} \begin{pmatrix} \Phi_{|n_+|-1, |n_-|-1}(\mathbf{r}) \\ i^{-\text{sgn}(n_-)} \Phi_{|n_+|-1, |n_-|}(\mathbf{r}) \\ i^{\text{sgn}(n_+)} \Phi_{|n_+|, |n_-|-1}(\mathbf{r}) \\ i^{\text{sgn}(n_+) - \text{sgn}(n_-)} \Phi_{|n_+|, |n_-|}(\mathbf{r}) \end{pmatrix},$$

where

$$\Phi_{n_1, n_2}(\mathbf{r}) = \frac{2^{-\frac{|l_z|}{2}}}{\sqrt{2\pi}} \frac{n_2!}{\sqrt{n_1! n_2!}} \frac{1}{r_B} \quad (5)$$

$$\times e^{-il_z \phi} \text{sgn}(l_z)^{l_z} \frac{r^{|l_z|}}{r_B^{|l_z|}} L_{n_1}^{|l_z|}(r^2/2r_B^2) e^{-r^2/4r_B^2}$$

with L denoting Laguerre polynomials $z = x + iy$, $l_z = n_1 - n_2$, $n_- = \min(n_1, n_2)$, $z/|z| = e^{i\phi}$, and $\text{sgn}(l_z)^{l_z} \rightarrow 1$ for $l_z = 0$.

When the inter-LL Coulomb interaction is taken into account, however, one should perform diagonalization of full Hamiltonian of Coulomb interacting carriers in some basis of magnetoexcitonic states $\Psi_{n_+, n_-}(r)$. In other words, to obtain eigenvalues of the Hamiltonian H , we need to numerically solve the following eigen-equation [34]:

$$0 = \det \left\| \delta_{n_+, n'_+} \delta_{n_-, n'_-} (E_{n_+, n_-}^{(0)} - E) \right. \quad (6)$$

$$\left. + \langle \Psi_{n'_+, n'_-} | U(\mathbf{r} - r_B^2 \hat{\mathbf{z}} \times \mathbf{P}) | \Psi_{n_+, n_-} \rangle \right\|.$$

The location of the chemical potential will determine the possible LL indices for electrons and holes. We should point out that the intra-LL component of the Coulomb interaction is defined as $\langle \Psi_{n_+, n_-} | U | \Psi_{n_+, n_-} \rangle$, while the inter-LL component is defined as $\langle \Psi_{n'_+, n'_-} | U | \Psi_{n_+, n_-} \rangle$, where $|\Psi_{n'_+, n'_-}\rangle \neq |\Psi_{n_+, n_-}\rangle$.

Consider a magnetoexciton is formed by an electron on the LL n and a hole on the LL m . In the limit of the relatively large separation D between electron and

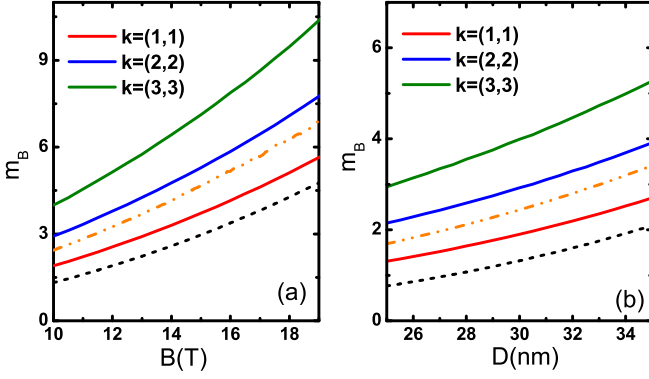


FIG. 2: (Color online) Calculated magnetoexciton effective mass m_B (in unit of free electron mass) as functions of (a) magnetic field B and (b) spacer width D , for different choices of magnetoexciton LL indices $k=(n,n)$. For comparison, the $k=(1,1)$ magnetoexciton effective mass without including inter-LL transition (given by Eq. (11)) is plotted by dash-dot-dotted lines and $m_B^{(0)}(D)$ given by Eq. (12) is shown by dashed lines. The spacer width in panel (a) is set as $D=30$ nm and the external magnetic field in panel (b) is set as $B=10$ T in (b). The other parameters are set as $v_F=3.0 \times 10^5$ m/s and $\epsilon=4.0$.

hole TIBs and relatively high magnetic field B when $e^2/(\epsilon D) \ll \hbar v_F/r_B$, the magnetoexciton energy can be approximated by only considering its zeroth order energy part $E_{n,m}^{(0)}$. However, at higher magnetic field $10 \sim 20$ T in experiment, the Coulomb interaction $e^2/(\epsilon D)$ is only several times less than the zeroth energy $\hbar v_F/r_B$. In this case, the Coulomb interaction can be treated as a perturbation, which could be departed into intra-LL part and inter-LL part. For the intra-LL part, the magnetoexciton energy can be written as

$$\begin{aligned}
 E_{n,m} &= E_{n,m}^{(0)} + \langle \Psi_{n,m} | U(\mathbf{r} - r_B^2 \hat{\mathbf{z}} \times \mathbf{P}) | \Psi_{n,m} \rangle \\
 &= E_{n,m}^{(0)} + 2^{\delta_{n,0} + \delta_{m,0} - 2} \\
 &\quad \times \{ \langle \langle |n| - 1, |m| - 1, \mathbf{P} | U | |n| - 1, |m| - 1, \mathbf{P} \rangle \rangle \\
 &\quad + \langle \langle |n| - 1, |m|, \mathbf{P} | U | |n| - 1, |m|, \mathbf{P} \rangle \rangle \\
 &\quad + \langle \langle |n|, |m| - 1, \mathbf{P} | U | |n|, |m| - 1, \mathbf{P} \rangle \rangle \\
 &\quad + \langle \langle |n|, |m|, \mathbf{P} | U | |n|, |m|, \mathbf{P} \rangle \rangle \}, \quad (7)
 \end{aligned}$$

where the notation $\langle \langle nmP | U | nmP \rangle \rangle$ denotes the averaging by the two-dimensional harmonic oscillator eigenfunctions $\Phi_{n,m}(r)$. Substituting for small magnetic momenta $P \ll \hbar/r_B$ and $P \ll \hbar D/r_B^2$ the relation

$$\langle \langle nmP | U | nmP \rangle \rangle = \mathcal{E}_{nm}^{(b)} + \frac{P^2}{2M_{nm}(B, D)} \quad (8)$$

into Eq. (7), we can get the dispersion law of a magnetoexciton for small magnetic momenta. As an example, let us consider the magnetoexciton on the $k=(1,1)$ LL. The magnetoexciton energy at small magnetic momenta

is then given by

$$E_{1,1}(P) = \mathcal{E}_B^{(b)}(D) + \frac{P^2}{2m_B(D)}, \quad (9)$$

where the binding energy $E_B^{(b)}(D)$ is expressed as

$$\mathcal{E}_B^{(b)}(D) = \frac{1}{4}E_{00}^{(b)} + \frac{1}{2}E_{01}^{(b)} + \frac{1}{4}E_{11}^{(b)} \quad (10)$$

and the effective magnetic mass $m_B(D)$ of a magnetoexciton is expressed as

$$\frac{1}{m_B} = \frac{1}{4M_{00}} + \frac{1}{2M_{01}} + \frac{1}{4M_{11}}. \quad (11)$$

Here, the constants $E_{00}^{(b)}$, $E_{01}^{(b)}$, $E_{11}^{(b)}$, M_{00} , M_{01} , and M_{11} depend on magnetic field B and the interlayer separation D . Explicitly, $E_{00}^{(b)} = -CE_0$, $E_{01}^{(b)} = -E_0[(\frac{1}{2}-x)C + \frac{x}{\sqrt{\pi}}]$, $E_{11}^{(b)} = -E_0[(\frac{3}{4} + x^2 + x^4)C - \frac{1}{\sqrt{\pi}}(\frac{x}{2} + x^3)]$, and $M_{00} = M_0[(1 + 2x^2)C - \frac{2x}{\sqrt{\pi}}]^{-1}$, $M_{01} = M_0[(3 + 2x^2)\frac{x}{\sqrt{\pi}} - (\frac{1}{2} + 4x^2 + 2x^4)C]^{-1}$, $M_{11} = M_0[\frac{C}{4}(7 + 50x^2 + 44x^4 + 8x^6) - (\frac{17}{2} + 10x^2 + 2x^4)\frac{x}{\sqrt{\pi}}]^{-1}$, with $x = D/(\sqrt{2}r_B)$, $E_0 = \frac{e^2}{\epsilon r_B} \sqrt{\frac{\pi}{2}}$, $M_0 = \frac{2^{3/2} \epsilon \hbar^2}{\sqrt{\pi} \epsilon^2 r_B}$, and functions $erfc(x)$ and $C(x)$ respectively defined as $erfc(x) = \frac{2}{\sqrt{\pi}} \int_x^{+\infty} \exp(-t^2) dt$ and $C(x) = e^{x^2} erfc(x)$. In the special limit of $D \gg r_B$, one obtains

$$m_B^{(0)}(D) = \frac{D^3 \hbar^2 \epsilon}{r_B^4 e^2}. \quad (12)$$

We should notice that the effective magnetic mass in the present system is equal to that in coupled semiconductor quantum wells at the same D , ϵ , and B , which is four times larger than that in graphene bilayers [11, 13]. Although the effective low-energy Hamiltonian of the electron-hole graphene bilayer system is also expressed as a 4×4 matrix, which is similar to Eq. (1) shown above, the momentum therein is actually coupled with the pseudospins of sublattices rather than the real spins of electron and hole. Therefore, the factor 1/4 in the effective magnetic mass of magnetoexcitons in graphene bilayer system arises from the spin degeneracy (see Fig. 1(b)), which is absent in the TIB system considered here since the freedom of spin has been involved due to the strong spin-orbit coupling in the original effective Hamiltonian Eq. (1). This significant difference between TIB and graphene bilayer may be detected by the gyromagnetic resonance experiments.

Now let us make a simple estimate to illustrate the reasonability of the perturbation theory. We choose the Fermi velocity and the electron-hole interlayer distance as $v_F = 3 \times 10^5$ m/s and $D = 30$ nm. The dielectric constant of the spacer SiO_2 is $\epsilon = 4.0$. Under these conditions, one can obtain the Coulomb interaction $e^2/(\epsilon D) = 12$ meV and kinetic energy $\hbar v_F/r_B = 24.4$ meV (corresponding to $r_B = 8.1$ nm) when the applied magnetic field $B = 10$ T.

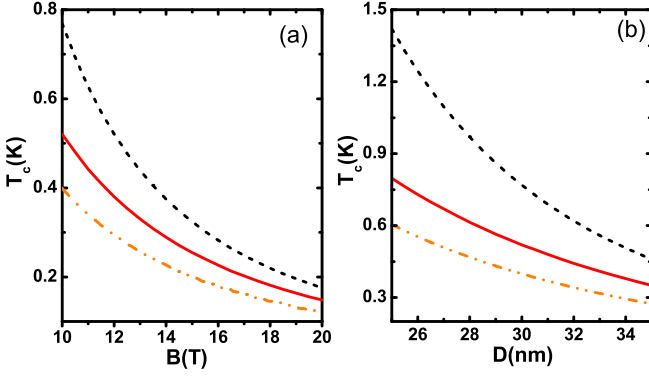


FIG. 3: (Color online) Calculated KT temperature versus (a) magnetic field and (b) spacer width. The density of magnetoexciton is set as $n=4.0 \times 10^{11} \text{ cm}^{-2}$. The spacer width $D=30 \text{ nm}$ is used in panel (a) and the magnetic field $B=10 \text{ T}$ is used in panel (b). The red solid, black dashed, and blue dotted lines correspond to the magnetoexciton effective mass obtained by considering both intra-LL and inter-LL Coulomb interaction, only intra-LL Coulomb interaction, and the approximation Eq. (12) at $D \gg r_B$, respectively.

In this case, $e^2/(\epsilon D)/(\hbar v_F/r_B) \simeq 0.5$, which indicates that in our studied TIB system, the effect of Coulomb interaction can be treated as a perturbation. Same analysis can also be applied to graphene, in which the Fermi velocity is about 3 times larger than that in Bi_2Se_3 film. With the same external parameters for estimation, one can immediately obtain $e^2/(\epsilon D)/(\hbar v_F/r_B) \simeq 0.17$ for graphene bilayer system. In the above calculations of the magnetoexciton energy and effective mass we only consider the intra-LL Coulomb interaction. On the other hand, the inter-LL Coulomb interaction is also important. We will show in the following that the inter-LL Coulomb interaction can bring about 0.15~0.25 times modification of the magnetoexciton effective mass (see Fig. 2).

To study the whole effect of Coulomb interaction, including the intra-LL and inter-LL Coulomb interaction, on the effective magnetoexciton mass as well as KT transition to the superfluid state, we have to numerically solve Eq. (6). In our numerical calculations we have used four electron and four hole levels around the LL $k = (n, n)$. Figures 2(a) and 2(b) respectively show the numerically calculated magnetoexciton mass $m_B(D)$ as a function of the magnetic field and the dielectric spacer width D with different LL indices k . To observe the effect of inter-LL Coulomb interaction, we also exhibit in both figures the magnetoexciton effective mass at LL $k = (1, 1)$ by dash-dotted lines without inter-LL transition [Eq. (11)], and the analytical approximation results of magnetoexciton mass $m_B^{(0)}$ [Eq. (12)] by dashed lines. Comparing these results, one can find that for the magnetic field strength $B = 10 \sim 20 \text{ T}$ and the spacer width $D = 25 \sim 35 \text{ nm}$, the magnetoexciton effective mass is reduced by 15% ~ 25% by the inclusion of the inter-LL Coulomb interaction.

III. SUPERFLUIDITY OF DIPOLE MAGNETOEXCITONS

The magnetoexcitons that are constructed by spatially separated electrons and holes in TIB at large interlayer separation $D \gg r_B$ form two-dimensional weakly non-ideal gas of bosons. This is valid, because we can think the indirect exciton interact as parallel dipoles when $D \gg r_B$. So at low temperatures, these magnetoexcitons condense in Bose-Einstein type and form superfluid state below the KT transition temperature T_c [35, 36], which is determined by

$$T_c = \frac{\pi \hbar^2 n_s(T_c)}{2k_B m_B}, \quad (13)$$

where $n_s(T)$ is the superfluid density of the magnetoexciton system and k_B is the Boltzmann constant.

To solve the superfluid density n_s in Eq. (13), we can first solve the normal density n_n because $n_s = n - n_n$, where n is the total density. Through the usual procedure [11, 37], we have the normal density n_n as

$$n_n = \frac{3\zeta(3) k_B^3 T^3}{2\pi \hbar^2 m_B c_s^4}, \quad (14)$$

where $\zeta(z)$ is the Riemann zeta function and $c_s = \sqrt{\mu/m_B}$ is the sound velocity with the chemical potential

$$\mu = \frac{\pi \hbar^2 n}{m_B \ln[\hbar^4 \epsilon^2 / (2\pi n m_B^2 e^4 D^4)]}. \quad (15)$$

Finally, combining Eqs. (13)-(15), we obtain the KT transition temperature

$$T_c = \left[\left(1 + \sqrt{\frac{32}{27} \left(\frac{m_B k_B T_c^0}{\pi \hbar^2 n} \right)^3 + 1} \right)^{1/3} - \left(\sqrt{\frac{32}{27} \left(\frac{m_B k_B T_c^0}{\pi \hbar^2 n} \right)^3 + 1} - 1 \right)^{1/3} \right] \frac{T_c^0}{2^{1/3}}, \quad (16)$$

where $T_c^0 = \frac{1}{k_B} \left(\frac{2\pi \hbar^2 n \mu^2}{3m_B \zeta(3)} \right)^{1/3}$ is an auxiliary quantity that is equal to the temperature at which the superfluid density vanishes in the mean-field approximation (i.e., $n_s(T_c^0) = 0$).

We calculate T_c for different choices of magnetic field (10 ~ 20 T), dielectric spacer width D (25 ~ 35 nm), and magnetoexciton density n (up to $1.0 \times 10^{12} \text{ cm}^{-2}$). The results are presented in Fig. 3 and Fig. 4. One can find the following features: (i) The KT temperature is up to several Kelvins in our calculated ranges, which is similar to that in graphene bilayer and coupled semiconductor quantum wells [11, 12]; (ii) Figure 3 clearly shows that the calculated T_c evidently depends on the effective magnetoexciton mass form. Comparing the T_c calculated with full Coulomb interaction (red lines) with that in the

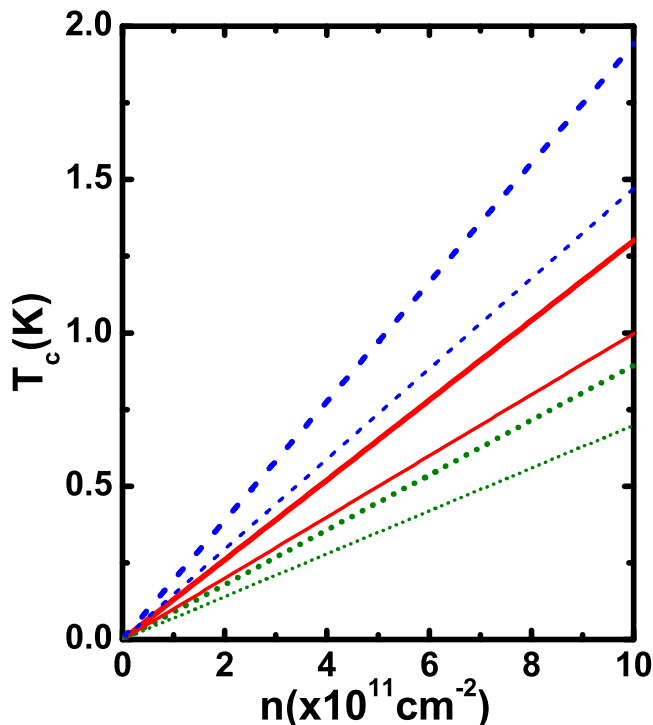


FIG. 4: (Color online) Calculated KT temperature versus magnetoexciton density n at $B=10$ T. The solid, dashed, and dotted curves correspond to $D=30, 25,$ and 35 nm, respectively. Here for comparison, the results with and without inter-LL Coulomb interaction included are given by thick and thin curves, respectively.

absence of inter-LL Coulomb interaction (orange lines), one can find that there is about 20%~25% correction induced by inter-LL Coulomb interaction. By decreasing the magnetic field or the dielectric spacer width, this correction becomes more prominent, which indicates that

the inter-LL transition caused by Coulomb interaction is significant in estimating T_c . When the magnetoexciton mass approximately takes the limit form Eq. (12) at $D \gg r_B$, the KT temperature has a promotion (black lines). Especially at relatively small values of B and D , this promotion becomes very remarkable and almost reaches 100%; (iii) Figure 4 shows T_c in good approximation linearly increases with increasing magnetoexciton density n . This is due to the fact that the denominator in Eq. (15) for the chemical potential and thus the sound velocity, weakly depends on n .

IV. CONCLUSION

In summary, we have theoretically studied the effective mass and KT transition temperature of magnetoexcitons in TIB structure under a strong perpendicular magnetic field. When only intra-LL Coulomb interaction is considered, the effective magnetoexciton mass in TIB structure is four times larger than that in graphene bilayer structure, while the calculated KT temperature is about several Kelvins, same in amplitude as in graphene bilayer and semiconductor bilayer systems. The inclusion of inter-Landau-level Coulomb interaction has been shown to bring about significant corrections to magnetoexciton properties by prominently reducing the magnetoexciton effective mass and promoting the KT temperature.

Acknowledgments

This work was supported by NSFC under Grants No. 90921003 and No. 10904005, and by the National Basic Research Program of China (973 Program) under Grant No. 2009CB929103.

-
- [1] Y.E. Lozovik and V.I. Yudson, Zh. Eksp. Teor. Fiz. **71**, 738 (1976) [Sov. Phys. JETP **44**, 389 (1976)].
 - [2] S.I. Shevchenko, Fiz. Nizk. Temp. **2**, 505 (1976) [Sov. J. Low Temp. Phys. **2**, 251 (1976)].
 - [3] D.W. Snoke, Science **298**, 1368 (2002).
 - [4] L.V. Butov, J. Phys.: Condens. Matter **16**, R1577 (2004).
 - [5] V.B. Timofeev and A.V. Gorbunov, J. Appl. Phys. **101**, 081708 (2007).
 - [6] J.P. Eisenstein and A.H. MacDonald, Nature (London) **432**, 691 (2004).
 - [7] C.H. Zhang and Y.N. Joglekar, Phys. Rev. B **77**, 233405 (2008).
 - [8] H. Min, R. Bistrizer, J.-J. Su, and A.H. MacDonald, Phys. Rev. B **78**, 121401(R) (2008).
 - [9] Y.E. Lozovik and A.A. Sokolik, Pis'ma Zh. Eksp. Teor. Fiz. **87**, 61 (2008).
 - [10] A. Iyengar, J.H. Wang, H.A. Fertig, and L. Brey, Phys. Rev. B **75**, 125430 (2007).
 - [11] O.L. Berman, Y.E. Lozovik, and G. Gumbs, Phys. Rev. B **77**, 155433 (2008).
 - [12] O.L. Berman, R.Ya. Kezerashvili, and Y.E. Lozovik, Phys. Rev. B **78**, 035135 (2008).
 - [13] Z.G. Koinov, Phys. Rev. B **79**, 073409 (2009).
 - [14] C. L. Kane and E. J. Mele, Phys. Rev. Lett. **95**, 226801 (2005); **95**, 146802 (2005).
 - [15] B.A. Bernevig, T.L. Hughes, and S.-C. Zhang, Science **314**, 1757 (2006).
 - [16] L. Fu and C. L. Kane, Phys. Rev. B **76**, 045302 (2007).
 - [17] M. König, S. Wiedmann, Christoph Brüne, A. Roth, H. Buhmann, L. W. Molenkamp, X.-L. Qi, and S. C. Zhang, Science **318**, 766 (2007).
 - [18] D. Hsieh, D. Qian, L. Wray, Y. Xia, Y. S. Hor, R. J. Cava, and M. Z. Hasan, Nature **452**, 970 (2008).
 - [19] H. J. Zhang, C. X. Liu, X. L. Qi, X. Dai, Z. Fang, and S. C. Zhang, Nature Phys. **5**, 438 (2009).
 - [20] Y. Xia, D. Qian, D. Hsieh, L. Wray, A. Pall, H. Lin, A.

- Bansil, D. Grauer, Y. S. Hor, R. J. Cava, *Nat. Phys.* **5**, 398 (2009).
- [21] Y. L. Chen, J. G. Analytis, J. H. Chu, Z. K. Liu, S. K. Mo, X. L. Qi, H. J. Zhang, D. H. Lu, X. Dai, Z. Fang, *Science* **325**, 178 (2009).
- [22] M.Z. Hasan and C.L. Kane, *Rev. Mod. Phys.* **82**, 3045 (2010), and references therein.
- [23] X.L. Qi and S.C. Zhang, *Rev. Mod. Phys.* **83**, 1057 (2011), and references therein.
- [24] J. W. Luo and A. Zunger, *Phys. Rev. Lett.* **105**, 176805 (2010).
- [25] Y. S. Hor, A. Richardella, P. Roushan, Y. Xia, J. G. Checkelsky, A. Yazdani, M. Z. Hasan, N. P. Ong, and R. J. Cava, *Phys. Rev. B* **79**, 195208 (2009).
- [26] C.-Z. Chang, K. He, L.-L. Wang, X.-C. Ma, M.-H. Liu, Z.-C. Zhang, X. Chen, Y.-Y. Wang, and Q.-K. Xue, *Spin* **1**, 21 (2011).
- [27] Z. Li, Y. Qin, Y. Mu, T. Chen, C. Xu, L. He, J. Wan, F. Song, M. Han, G. Wang, *J. Nanosci. Nanotechnol.* **11**, 7042 (2011).
- [28] H. Liu and P.D. Ye, *Appl. Phys. Lett.* **99**, 052108 (2011).
- [29] R. Valdés Aguilar, A.V. Stier, W. Liu, L.S. Bilbro, D.K. George, N. Bansal, L. Wu, J. Cerne, A.G. Markelz, S. Oh, and N.P. Armitage, *Phys. Rev. Lett.* **108**, 087403 (2012).
- [30] H. D. Li, Z. Y. Wang, X. Guo, T. L. Wong, N. Wang, and M. H. Xie, *Appl. Phys. Lett.* **98**, 043104 (2011).
- [31] Z. Y. Wang, X. Guo, H. D. Li, T. L. Wong, N. Wang, and M. H. Xie, *Appl. Phys. Lett.* **99**, 023112 (2011).
- [32] B. Seradjeh, J.E. Moore, and M. Franz, *Phys. Rev. Lett.* **103**, 066402 (2009).
- [33] N. Hao, P. Zhang, and Y. Wang, *Phys. Rev. B* **84**, 155447 (2011).
- [34] Y.E. Lozovik and A.A. Sokolik, arXiv: 1111.1176 (2011).
- [35] J.M. Kosterlitz and D.J. Thouless, *J. Phys. C* **6**, 1181 (1973).
- [36] D.R. Nelson and J.M. Kosterlitz, *Phys. Rev. Lett.* **39**, 1201 (1977).
- [37] A.A. Abrikosov, L.P. Gorkov, and I.E. Dzyaloshinski, *Methods of Quantum Field Theory in Statistical Physics* (Prentice-Hall, Englewood Cliffs, NJ, 1963).